THE JOURNAL OF PHYSICAL CHEMISTRY C

ARTICLE

pubs.acs.org/JPCC

Nanoscale Structure Evolution in Alkoxide−Carboxylate Sol−Gel Precursor Solutions of Barium Titanate

Tomasz M. Stawski,[†] Sjoerd A. Veldhuis,[†] Rogier Besselink,[†] Hessel L. Castricum,[‡] G. Portale,[§] Dave H. A. Blank,[†] and Johan E. ten Elshof[†,*]

[†]MESA[+] Institute for Nanotechnology, University of Twente, P.O. Box 217, 7500 AE Enschede, The Netherlands

[‡]Van't Hoff Institute for Molecular Sciences, University of Amsterdam, Science Park 904, 1098 XH Amsterdam, The Netherlands

[§]Netherlands Organization for Scientific Research, DUBBLE@ESRF, BP 220, Grenoble F38043, France

ABSTRACT: The evolution of hydrolyzed alkoxide−carboxylate sol−gel precursor solutions of barium titanate was investigated by time-resolved small-angle X-ray scattering (SAXS) and viscosity measurements. Sols were prepared from titanium(IV) *iso*-propoxide in 2-methoxyethanol and barium acetate in acetic acid. Analysis of the experimental data showed that the evolution of the sol went through three stages. In stage (i) mainly isolated primary scatterers of ∼0.45 nm radius formed. Stage (ii) showed the growth of branched oligomeric mass fractal-like structures with a 3−15 nm gyration radius and fractal dimension 1.9−1.5, as well as the presence of internally ordered structures with a correlation length of ∼1.8 nm. In stage (iii), higher-level hierarchy developed in the sol, probably due to cluster−cluster aggregation of the fractal-like branched oligomers into a gel. The data suggest that the agglomerates of primary scatterers are Ti-based and are built of small spherical primary particles of very similar size. The inorganic core of these particles had a radius of ∼0.45 nm, and they had an outer organic ligand shell of ∼0.45 nm thickness. Ba-related species remained dissolved in the acetic acid matrix and were present as ions. No Ba-related species could be seen with SAXS. Ba seemed to exert an indirect influence on the growth and precipitation or stabilization of the titanium-based structures from solution.

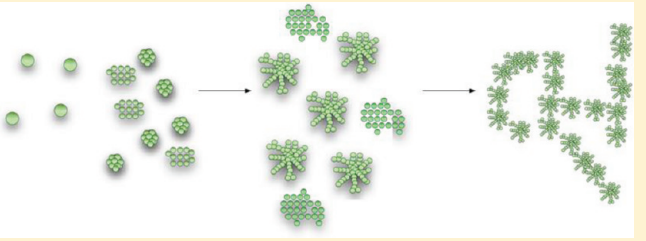

1. INTRODUCTION

Barium titanate ($BaTiO_3$) is a high-*k* dielectric material used in commercial multilayer ceramic capacitors. The minimum $BaTiO_3$ layer thickness that can be achieved with state of the art tape casting methods is about 1 μm, which implies the use of starting powders with a particle size of ca. 200 nm.[1] Further reduction of the barium titanate layer thickness requires finer powders obtained by new synthesis and deposition techniques.

Barium titanate synthesis methods developed in the last decades can be divided into (1) solid precursor-based methods (e.g., mixed oxide method and citrate route) and (2) wet-chemical methods, e.g., sol−gel, alkoxide−hydroxide sol precipitation, and hydrothermal route. In both groups, substantial progress was made, as can be seen by comparing the review of Pithan et al. from 2005[2] with that of Phule and Risbud from 1990.[3]

Wet-chemical methods provide nanometer-sized powders (5−100 nm) of high purity and homogeneity and of adjustable composition, as near-atomic level mixing of components is possible. Among these methods, the sol−gel process, in particular the alkoxide−carboxylate synthesis, the double alkoxide synthesis, the microemulsion synthesis, and the precipitation methods (alkoxide−hydroxide sol precipitation), received much attention.[2] Furthermore, as the sol−gel process is based on liquid precursors, direct deposition of amorphous precursor thin films onto substrates by means of spin-casting, deep-casting, or misted source deposition, followed by pyrolysis and crystallization, is possible.[4−6]

The alkoxide-carboxylate route has been employed widely for $BaTiO_3$ synthesis since the first reports by Phule and Risbud in 1988.[7] Barium titanate xerogels were synthesized from titanium(IV) *iso*-propoxide in *iso*-propanol and barium acetate in acetic acid. Acetic acid was used as a solvent, enabling the complete dissolution of barium acetate. Acetic acid is also known to chelate metal centers in alkoxides, leading to the formation of oligomeric metal oxoacetates.[5,8−11] This approach was further extended to other oxide precursor systems, such as barium strontium titanate, lead zirconate titanate, and lead lanthanum zirconate titanate.[4,5] The influence of precursor chemistry and processing conditions on the morphology of crystalline thin films processed from sol−gel was also investigated.[12,13] Use of acetic acid or propionic acid favored the growth or larger grains and yielded higher density barium titanate films in comparison with films synthesized from 2-ethylhexanoate-based precursors. The difference was attributed to the higher pyrolysis temperature of the system containing the shorter carboxylic acid, leading to formation of the transition oxocarbonate phase, $Ba_2Ti_2O_5CO_3$.[14] As a result, crystallization occurred at higher temperatures, which led to increased density of thin films and to larger grains. The morphology of crystalline barium strontium titanate and barium

Received: July 11, 2011
Revised: September 13, 2011
Published: September 14, 2011

titanate films derived from the alkoxide−carboxylate route could also be modified.[13] When the sol concentration was sufficiently low for a given composition of precursors, provided that films were deposited in a number of steps and crystallized after each deposition, columnar grains were formed. Above a certain threshold concentration, only a granular morphology was observed.

The stabilization of titanium alkoxide precursors is believed to play an important role, as it can modify the hydrolysis and condensation pathways. Hasenkox et al. noted that application of titanium alkoxide stabilized with acetylacetone resulted in denser films with larger grain sizes and better dielectric properties, which was attributed to the monomeric character of the titanium precursor and the homogeneous mixing of Ti and Ba precursors on the nanometer scale.[8] The authors hypothesized that in the case of nonstabilized solutions an oligomeric TiO_x phase might form, and the extent of phase formation would depend on the extent of oligomerization of the Ti alkoxide derived structure and chemical gel formation. The structure of such an alkoxide−carboxylate gel was proposed by Hennings et al.[4,15] based on transmission electron microscopy (TEM), energy disperse spectroscopy (EDS), and infrared spectroscopy (FT-IR) analysis. Metal carboxylate species were assumed to adsorb at the surface of the titanium oxoacetate polymer.[15] The separation between Ti-rich and Ba-rich regions exceeded 100 nm.

The properties of alkoxide−carboxylate derived thin films are therefore probably controlled by separation between immiscible or partly immiscible Ti-oxoacetate and Ba-carboxylate-rich domains. The separation is determined by, e.g., carboxylic acid chemistry, sol concentration, and chelating/stabilization agents. No details of nanoscale separation or of the structure of TiO_x oligomers in contact with metal carboxylates have been reported to our knowledge. It was the aim of this work to obtain a better understanding of the evolution of nanostructure in hydrolyzed model solutions of titanium alkoxide and barium acetate in acetic acid. We employed time-resolved small-angle X-ray scattering (SAXS) to study the structural evolution in this system on a nanometer scale. In the next section, a model is derived to which the experimental SAXS data could be fitted. The model is based on the assumption that hydrolysis yields two types of structures in solution distinguishable by X-ray scattering, namely, (i) mass fractal-like structures and (ii) structures with internal correlations. Both structure types are thought to be assembled from similar spherical primary scatterers, and they seem not to interact in solution. In terms of sol−gel chemistry, the fractal-like structures can be associated with branched oligomeric species dissolved in a solvent matrix, and the structures with internal correlations resemble dense agglomerates of primary particles (precipitates).

In addition to SAXS, we also used viscosity measurements as a function of time and temperature to monitor the global changes in the solution and locate the main transitions of the process. Gelation of the system was promoted by hydrolysis of the barium titanate precursor sol with varying concentrations of water, which enabled us to follow the extent of oligomer growth by time-resolved SAXS.

2. SCATTERING MODEL

In a typical SAXS experiment, the scattering intensity $I(q)$ is plotted versus the scattering vector q (nm^{-1}), which is related to the scattering angle θ and the wavelength λ (nm) of the incident beam via[16−19]

$$q = 4\pi/\lambda \sin\theta \tag{1}$$

The amplitude of the form factor of a homogeneous sphere, $F(q)$, of radius r_0 is given by eq 2[16−18]

$$F(q, r_0) = \frac{3[\sin(qr_0) - qr_0\cos(qr_0)]}{(qr_0)^3} \tag{2}$$

The scattered intensity $I(q)$ from the dilute system of noninteracting, monodisperse, homogeneous spherical particles of number density N, with electron density difference between the particles and the surrounding medium (scattering contrast) $\Delta\rho$ and particle volume V can be expressed by eq 3, where $P(q)$ is the form factor.

$$\begin{aligned} I(q) &= N(\Delta\rho)^2V^2F^2(q, r_0) \\ &= N(\Delta\rho)^2\left(V\frac{3[\sin(qr_0) - qr_0\cos(qr_0)]}{(qr_0)^3}\right)^2 \\ &= N(\Delta\rho)^2P(q) \end{aligned} \tag{3}$$

Equation 3 is insufficient to describe systems with a higher concentration of particles, as it neglects the interference terms due to interactions between particles, such as Coulomb repulsion−attraction phenomena, agglomeration and clustering effects, or spatial correlations within the system.[20,21] These can be included by introducing the structure factor, $S(q)$

$$I(q) = N(\Delta\rho)^2P(q)S(q) \tag{4}$$

2.1. Mass Fractal-Like Particles. Primary particles can cluster and form branched oligomers, which may be described in terms of the well-established mass-fractal models.[22−24] A fractal-like particle is defined here as an object whose radius of gyration, R_g, is related to the number of primary particles n of which the particle is constructed, via eq 5[22−25]

$$n = k_0\left(\frac{R_g}{r_0}\right)^D \tag{5}$$

Here D is the so-called fractal dimension; r_0 is the radius of a primary particle of the fractal-like agglomerate; and k_0 is a constant. For true fractals, the parameter D expresses the dimensionality of the system, and its value can vary from 1 to 3. For real systems with a fractal-like structure, such as branched inorganic polymers, complex clusters; and other growing sol components, D is merely a fit factor that is associated with the internal shape and structure of the system under investigation. Its value is also generally found to be between 1 and 3. Fractals have a cutoff distance, ξ, and a characteristic length scale, above which the mass distribution in the structure no longer follows eq 5. They can be described by $S_F(q)$[23−25]

$$S_F(q) = 1 + \frac{D\Gamma(D-1)\sin[(D-1)\arctan(q\xi)]}{(qr_0)^D\left[1 + \frac{1}{(q^2\xi^2)}\right]^{(D-1)/2}} \tag{6}$$

The radius of gyration R_g of a fractal-like structure is related to cutoff distance ξ by eq 7[23−25]

$$R_g^2 = D(D + 1)\xi^2/2 \quad (7)$$

The mass-fractal structure factor is certainly valid when $r_0 \ll \xi$. This implies that very small entities composed of only a few primary particles cannot be described sufficiently well in terms of the model because they do not exhibit self-similar behavior over a range of length scales. In our study, such clusters are typically present at the beginning of sol−gel reactions. When the structures are very small and not mass fractal-like, the Guinier approximation can be used to determine R_g.[16] For $qR_g < 1$, the following approximation is valid independent of particle shape (11)

$$I(q) = N(\Delta\rho)^2V^2 \exp(-q^2R_g^2/3) \quad (8)$$

2.2. Structures with Internal Correlations. Systems composed of spherical primary particles of similar size can also form nonfractalic partially ordered correlated structures.[26] Such systems can also be approximated by hard-sphere potentials and be described by structure factor models based on the Percus−Yevick approximation.[27−29] They describe a system in terms of a volume fraction v of interacting particles with hard-sphere radius R_{HS}. The volume fraction is defined as the averaged volume fraction of particles, located at a distance $2R_{HS}$ from another particle.

$$S_C(q) = \frac{1}{1 + 24vG(qR_{HS})/(qR_{HS})}$$

$$G(qR_{HS}) = \frac{\alpha[\sin(qR_{HS}) - qR_{HS}\cos(qR_{HS})]}{(qR_{HS})^2} + \beta\left[2qR_{HS}\sin(qR_{HS}) + (2 - (qR_{HS})^2)\cos(qR_{HS}) - \frac{2}{(qR_{HS})^3}\right] + \gamma\left[-(qR_{HS})^4\cos(qR_{HS}) + 4[3(qR_{HS})^2 - 6]\cos(qR_{HS}) + 4[(qR_{HS})^3 - 6(qR_{HS})]\sin(qR_{HS}) + 24\right] \Big/ \left[(qR_{HS})^5\right]$$

$$\alpha = (1 + 2v)^2/(1 - v)^4 \qquad \beta = -6v(1 + v/2)^2/(1 - v)^2 \qquad \gamma = v\alpha/2 \quad (9)$$

2.3. Double Structure Factor Model. We assume that the systems under investigation are initially composed of nonagglomerated, identical spherical particles that formed upon hydrolysis. The scattered intensity is described by eq 4. As the system evolves, mass-fractal-like agglomerates characterized by a fractal dimension D and cutoff distance ξ, as defined by eq 6, start to form. It is noted that such fractal models do not describe small clusters that are formed in the earliest stages of a sol−gel process well.

On the other hand, we assume ordered structures with internal correlations that can be described in terms of eq 9. Hence, both $S_F(q)$ and $S_C(q)$ are present in $I(q)$, and they originate from physically and spatially different species. Provided that these two types of structures have no or very little interaction, a weight factor $0 < \varepsilon < 1$ can be defined to express the relative contribution to scattering intensity by fractal-like agglomerates. The scattered intensity of such a system, as a function of time, t, is given by eq 10

$$I(q,t) = N(\Delta\rho)^2P(q,t)[\varepsilon(t)S_F(q,t) + (1 - \varepsilon(t))S_C(q,t)] \quad (10)$$

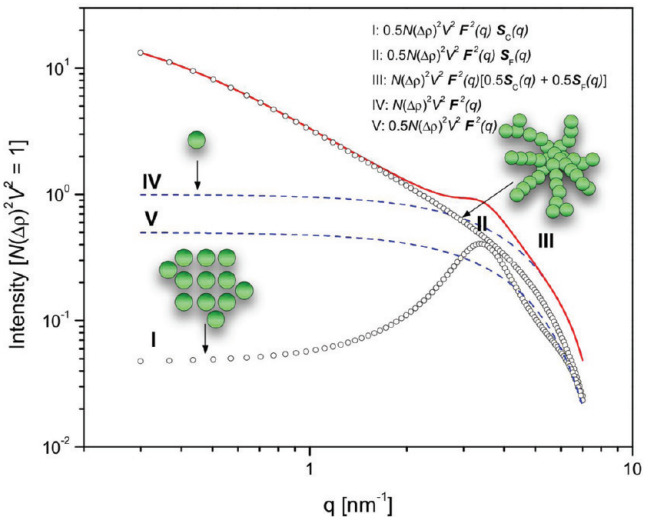

Figure 1. Simulated SAXS curves using eqs 3 and 10, with $N(\Delta\rho)^2V^2$ set to 1.0. (I) $I(q)$ of internally correlated structure with $r_0 = 0.5$ nm, $v = 0.3$, $2R_{HS} = 1.8$ nm, and $\varepsilon = 0.5$. (II) $I(q)$ of fractal-like structure with $r_0 = 0.5$ nm, $D = 1.8$, $\xi = 3$ nm (R_g =4.76 nm), and $\varepsilon = 0.5$. (III) $I(q)$ of linear combination of structures I and II. (IV) $I(q)$ of sphere form factor of $r_0 = 0.5$ nm. (V) $I(q)$ of sphere form factor of $r_0 = 0.5$ nm and $\varepsilon = 0.5$.

Here the intensity prefactor $\varepsilon(t)N(\Delta\rho)^2$ refers to primary particles with form factor $P(q)$ that are part of the mass fractal-like agglomerates that can be described in terms of the structure factor $S_F(q)$. The factor $(1 - \varepsilon(t))N(\Delta\rho)^2$ refers to the scattering contribution of structures that can be described by the structure factor $S_C(q)$. A few examples of scattering curves that can be simulated by eq 10 are presented in Figure 1. Equation 11 was used to fit all experimental SAXS data using the Levenberg−Marquardt algorithm.[30,31] We used $S_F(q)$ and $S_C(q)$ as defined by eqs 6 and 9, respectively. We also attempted to fit the experimental data under the more general assumption that these two types of structures may be interacting, but this did not result in good fits to the data.

3. EXPERIMENTAL SECTION

3.1. Synthesis of Barium Titanate (BTO) Precursor Sols. Barium acetate (>99%, Riedel-deHaën) and titanium(IV) *iso*-propoxide (99.999%, Sigma-Aldrich) were used as precursors. Glacial acetic acid (99.8%, Acros) and 2-methoxyethanol (>99.3%, Sigma-Aldrich) were used as solvents, stabilizers, and chelating agents. Two stock solutions were made. Barium acetate solution was prepared by dissolving barium acetate in acetic acid and refluxing at 105 °C for 8 h to remove all remaining water. The final concentration was adjusted to 1.0 mol/dm^3 by dilution with acetic acid. The second stock solution was based on 1.0 mol/dm^3 titanium *iso*-propoxide in 2-methoxyethanol and was prepared in a glovebox under nitrogen atmosphere. All stock solutions were stirred at room temperature for 24 h. They were then stored at room temperature. Prior to the experiments, the stock solutions were mixed in 1:1 molar ratios and stirred for 5 min, yielding a concentration of 0.50 mol/dm^3 in the final BTO precursor solution. Solutions of this concentration were used in all experiments. Hydrolysis was initiated by addition of water immediately after the two stock solutions had been mixed and stirred. Sols with hydrolysis ratios $[H_2O]/[Ti]$ of 2.8, 5.5, 16.7, 25, and 33 were investigated.

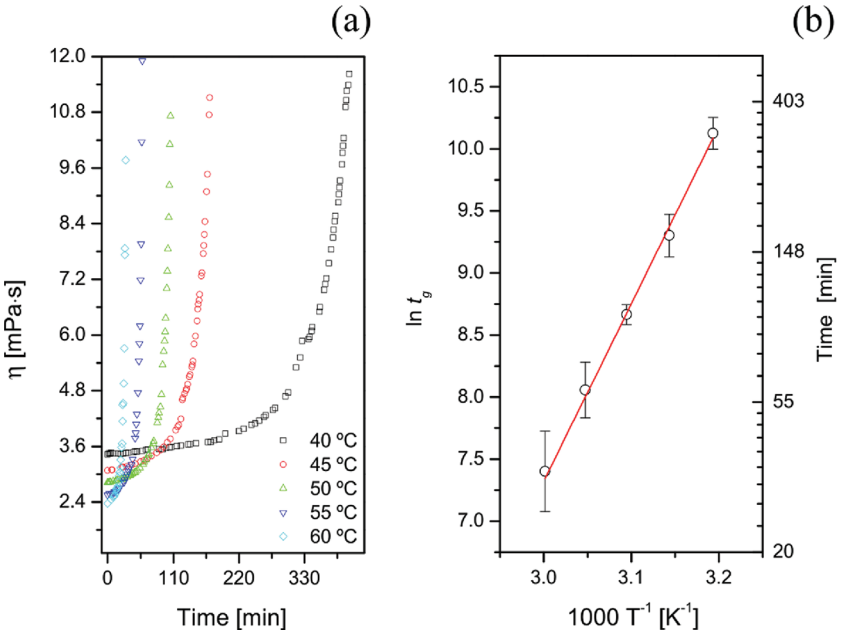

Figure 2. (a) Viscosity of a 0.5 M barium titanate precursor sol with $[H_2O]/[Ti]$ = 16.7 as a function of time and temperature. (b) Arrhenius-type representation based on gelation times at different temperatures. Gelation times were used as kinetic parameters to describe the rate of the sol−gel process (in s).

3.2. Viscosity Measurements. The viscosity of BTO precursor sols as a function of time was measured at 40−60 °C, using an Anton Paar AMVn-HT rolling-ball viscometer. For all the measurements, a glass capillary (Ø = 3.00 mm) was used, together with a steel ball (Ø = 2.5 mm) with a density of 7.71 g/cm^3. The setup was calibrated using the Anton Paar SH C120 calibration standard.

3.3. Small-Angle X-ray Scattering. SAXS experiments were performed on the Dutch-Belgian beamline (DUBBLE) BM-26B at the ESRF in Grenoble, France.[31] The beam was focused at the corner of a 2D gas-filled multiwire proportional CCD detector to maximize the range of accessible q values (scattering vector values). The beam energy was 16 keV (λ = 0.0776 nm). The samples were placed at a distance of 1.5 m from the detector, and the intensity was measured in the range $0.13 < q < 9.00$ nm^{-1}. The raw data were corrected for the pixel-dependent detector sensitivity and integrated for channels with the same q values. To investigate the in situ evolution of BTO precursor sols in situ at elevated temperatures, SAXS data were collected on sols in borosilicate glass sealed capillaries (Ø = 1.0 mm, glass no. 14, Hilgenberg, Malsfeld, Germany) that were mounted into a Linkam oven for capillaries, which was operated at 60 °C. Measurements were performed with 5 min intervals over a period of typically 1−3 h.

4. RESULTS AND DISCUSSION

4.1. Viscosity Measurements. Figure 2A shows the change in viscosity η as a function of time at different temperatures for a precursor sol with $[H_2O]/[Ti]$ = 16.7. The behavior of this system is typical for sols within the whole range of investigated hydrolysis ratios. The gelation time t_g was determined as a function of temperature. Assuming Arrhenius-type behavior for the temperature dependency, the experimental data points can be fitted by linear regression to

$$\ln t_g = E_a/RT + \text{const} \quad (11)$$

where E_a is the activation energy. Figure 2B depicts this dependence as ln t_g vs T^{-1}. The obtained activation energy was ca. 120 kJ/mol.

The data were also fitted to the Mass Fractal Growth (MFG) model.[32,33] In this model, the viscosity changes in a gel with a mass-fractal type growth regime follow eq 12

$$\ln(\eta/\eta_0 - 1) = \text{const} + q_r(3 - D)t \quad (12)$$

where η_0 is the viscosity of the solvent medium, q_r a rate constant, and D the fractal dimension. Figure 3A presents plots of the relative viscosity change $\ln(\eta/\eta_0 - 1)$ as a function of t/t_g for selected temperatures. In view of eq 12, a linear relationship between viscosity and time is expected in the period at which mass-fractal branched agglomerates develop ($D > 1$). As Figure 3A shows, a linear relationship was found in the range $0.2 < t/t_g < 0.8$. Data collected at other temperatures exhibited similar trends. The rate of reaction was highest at 60 °C, and due to the limited time resolution of the viscometer, only data for $t/t_g > 0.2$ could be monitored at that particular temperature.

The regime $t/t_g < 0.2$ did not follow eq 12, showing that other growth modes were present. The trends may be explained in terms of the presence of small agglomerates in which branching is not yet profound.

Equation 12 no longer holds at $t/t_g > 0.8$, suggesting that the mechanism of growth changes and one or more processes other than mass-fractal growth become dominant. Probably, $t/t_g = 0.8$ marks the onset of hierarchical aggregation of fractal-like particles, leading to the formation of the physical gel network.[32−34]

In the Near-Linear Growth model (NLG), it is assumed that the viscosity of a near-linear polymer is related to its molecular weight M by Flory's eq 13.[35] The evolution of $M(t)$ with time t can be parametrized by f, which is defined as the number of functional groups of the monomer.[36,37]

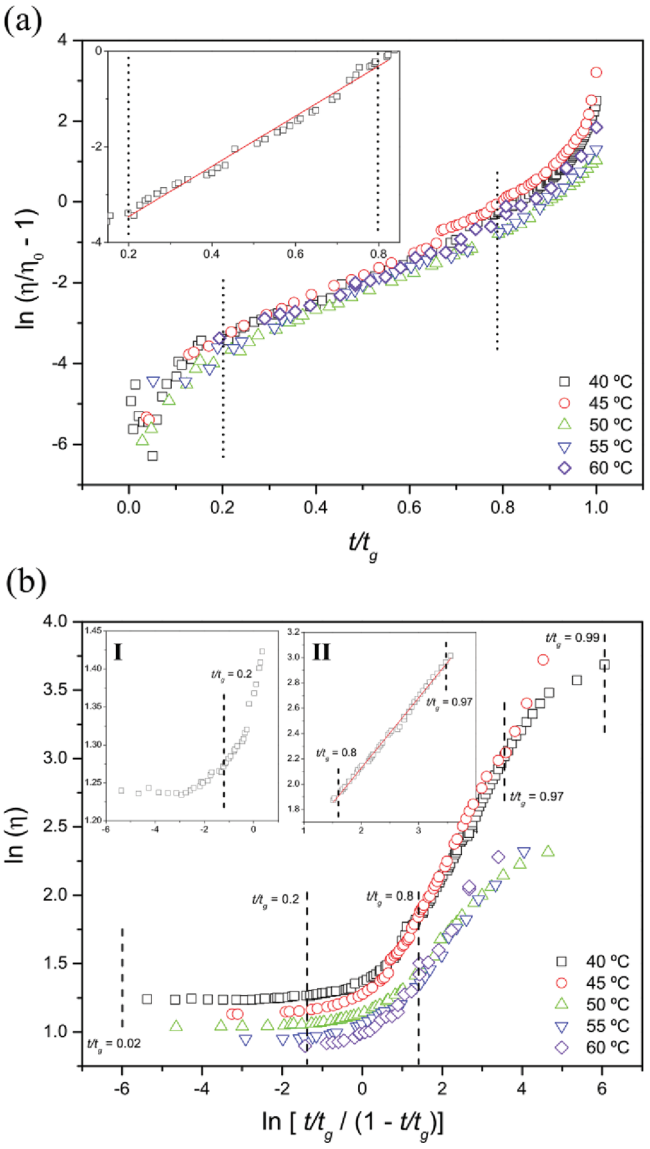

Figure 3. (a) MFG model representation of viscosity of sol with $[H_2O]/[Ti]$ = 16.7: $\ln(\eta/\eta_0 - 1)$ as a function of t/t_g at different temperatures. Inset presents measurement at 40 °C with a linear fit for $0.2 < t/t_g < 0.8$ (correlation coefficients $R^2 > 0.99$). (b) NLG model representation: $\ln \eta$ as a function of $\ln[t/t_g/(1 - t/t_g)]$ at different temperatures. Inset I presents measurement at 40 °C for $t/t_g < 0.2$. Inset II represents the measurement at 40 °C with a linear fit in the range $0.8 < t/t_g < 0.97$ (correlation coefficient $R^2 > 0.99$).

The relevant equations read

$$\ln(\eta) = \text{const} + m \ln M(t) \tag{13}$$

$$\frac{M(t)}{M(0)} = \frac{(f-2) + 2(t/t_g)}{(f-2)[1-(t/t_g)]} \tag{14}$$

Here m is a constant, and $M(0)$ is the molecular weight of the monomer. It can be shown that when f is slightly larger than 2 in the NLG regime eq 15 is valid[35−37]

$$\ln \eta = \text{const} + m \ln \frac{2M(0)}{f-2} + m \ln\left(\frac{t/t_g}{1-t/t_g}\right) \tag{15}$$

Linear growth can be visualized by a straight line in the plot of $\ln(\eta)$ versus $\ln[t/t_g/(1 - t/t_g)]$. The linear dependence does not hold for $t/t_g < 0.2$, as can be seen in inset I of Figure 3B. However, the linear trend in inset II in Figure 3B shows that the NLG model does fit the trend for $0.8 < t/t_g < 0.97$. This is the region in Figure 3A that, we think, is dominated by hierarchical aggregation of fractal-like structures. Description within NLG does not necessarily imply that the actual aggregates are linear but that they are of relatively low density. The fractal-like particles from which the aggregate is constructed have only two or slightly more than two neighbors. Such a gel structure agrees well with the model proposed by Pope and Mackenzie,[32] and completely analogous behavior was also observed upon gelation of a barium hydroxide−titanium isopropoxide in 2-methoxyethanol BTO precursor system.[33]

4.2. Time-Resolved SAXS of Hydrolyzed Barium Titanate Precursor Sols. The structural evolution in 0.5 mol/dm^3 barium titanate precursor sols with varying hydrolysis ratios was monitored by SAXS at 60 °C for periods of 60−180 min. Time-resolved scattering curves of sols with hydrolysis ratios between 5.6 and 33 are shown in Figure 4A−D.

An example of fits of eq 10 to experimental SAXS curves is presented in Figure 4E, where a sol with $[H_2O]/[Ti]$ = 16.7 after 5−60 min of reaction is shown. Best fits of parameters characterizing all sols as a function of time are presented in Figures 5−7.

Figure 5A shows the evolution of r_0 as a function of time for several hydrolysis ratios. In all investigated sols, this parameter increased slightly as the sol−gel reaction progressed and reached a plateau around the same value, independent of hydrolysis ratio. For the sol with $[H_2O]/[Ti]$ = 5.6, growth of r_0 from 0.43 to 0.46 nm occurred during the first 20 min of the process. The general trends suggest that the primary particles that were formed were fairly identical in all systems.

Figure 5B depicts the evolution of D. For the sol with $[H_2O]/[Ti]$ = 5.6, D could be accurately established from fitting routines after the 25th minute of the process. During the first 20 min, small agglomerates were formed, with $D = 3 \pm 1$ (not shown here) within experimental error. After this first period, the value of D decreased from 2.7 until it reached a constant value of 1.9−2.0. The first determinable values of D were smaller at higher hydrolysis ratios, with final values of 1.4−1.7 for $[H_2O]/[Ti]$ = 16.7−33, after 30 min of reaction.

The evolution of the gyration radii of the fractal-like structures, calculated from ξ using eq 6, is shown in Figure 5C. Since fractal-like structures were not formed yet, the first four data points in the plot of the sol with the lowest hydrolysis ratio were calculated using the Guinier approximation, eq 7. The scattering data of that sol are plotted as $\ln I(q)$ vs q^2 for $q < R_g^{-1}$ (see inset in Figure 5C). The radii of gyration increased from 0.6 nm up to a constant value of ca. 3.1 nm. In general, R_g increased with hydrolysis ratio. For $[H_2O]/[Ti]$ = 25, R_g grew from ca. 1.8 nm to a constant value of 7.5 nm. In the sol with $[H_2O]/[Ti]$ = 33, they grew from 3.3 to ∼20 nm after 30 min. In the latter two sols, a maximum in R_g, accompanied by an inflection point in the value of D, could be observed after approximately 30 min.

Figure 6 shows the evolution of the parameters for correlation length and packing density in the structures with internal correlations. The development of this correlation is illustrated in detail in inset I of Figure 6A, where data of a BTO sol with $[H_2O]/[Ti]$ = 16.7 are shown. The structure factor manifested itself as a wide maximum around q_{max} = 3.3 nm^{-1}. This corresponds to a

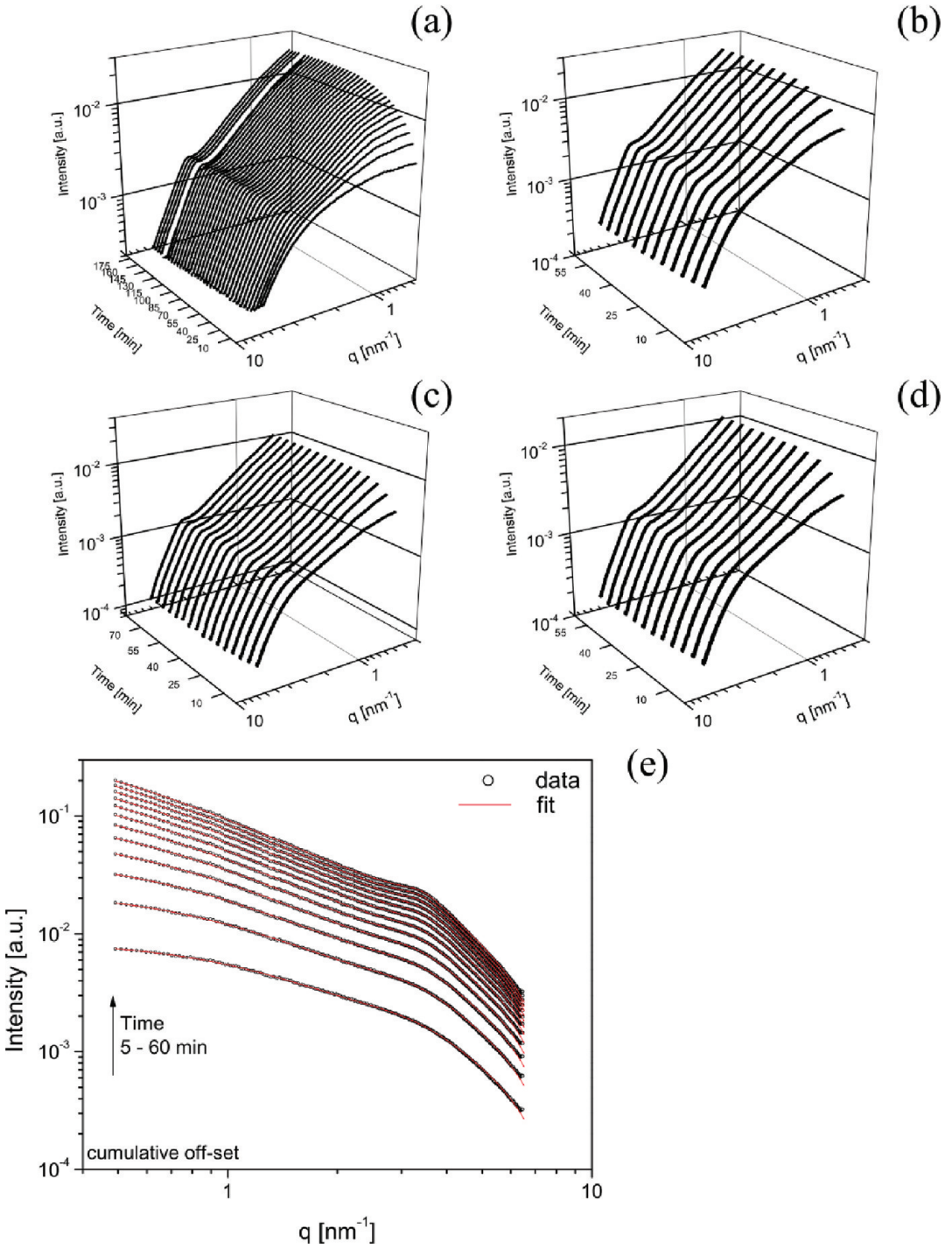

Figure 4. Time-resolved SAXS patterns at 60 °C, showing evolution of barium titanate precursor sols of initial 0.5 mol/dm^3 concentration with varying hydrolysis ratio. (a) $[H_2O]/[Ti]$ = 5.6, (b) $[H_2O]/[Ti]$ = 16.7, (c) $[H_2O]/[Ti]$ = 25.0, (d) $[H_2O]/[Ti]$ = 33.0. (e) Scattering curves of sol with $[H_2O]/[Ti]$ = 16.7 with best fits based on eq 11.

dimension of $2\pi/q_{max}$ = 1.9 nm in real space. The scattering maximum shifted to lower q-values as the system developed, indicating minimal growth. However, the intensity of the correlation peak increased, which is indicative of an increasing degree of order in the structural feature from which the correlation originated. The hard-sphere diameter $2R_{HS}$ was 1.8−1.9 nm and increased only slightly (Figure 6A), while the average volume fraction of hard spheres v at a distance $2R_{HS}$ around an arbitrary sphere (a measure for packing density) increased from 10% to 40% (Figure 6B).

Figure 7 depicts the evolution of parameters $N(\Delta\rho)^2$ and ε. The intensity factor related to the fractal-like structures is $\varepsilon N(\Delta\rho)^2$, and the intensity factor of the internally correlated structures is $(1 - \varepsilon)N(\Delta\rho)^2$. Due to the fact that samples were measured in capillaries with slightly varying dimensions, the intensity is shown in arbitrary units. Absolute values of $N(\Delta\rho)^2$

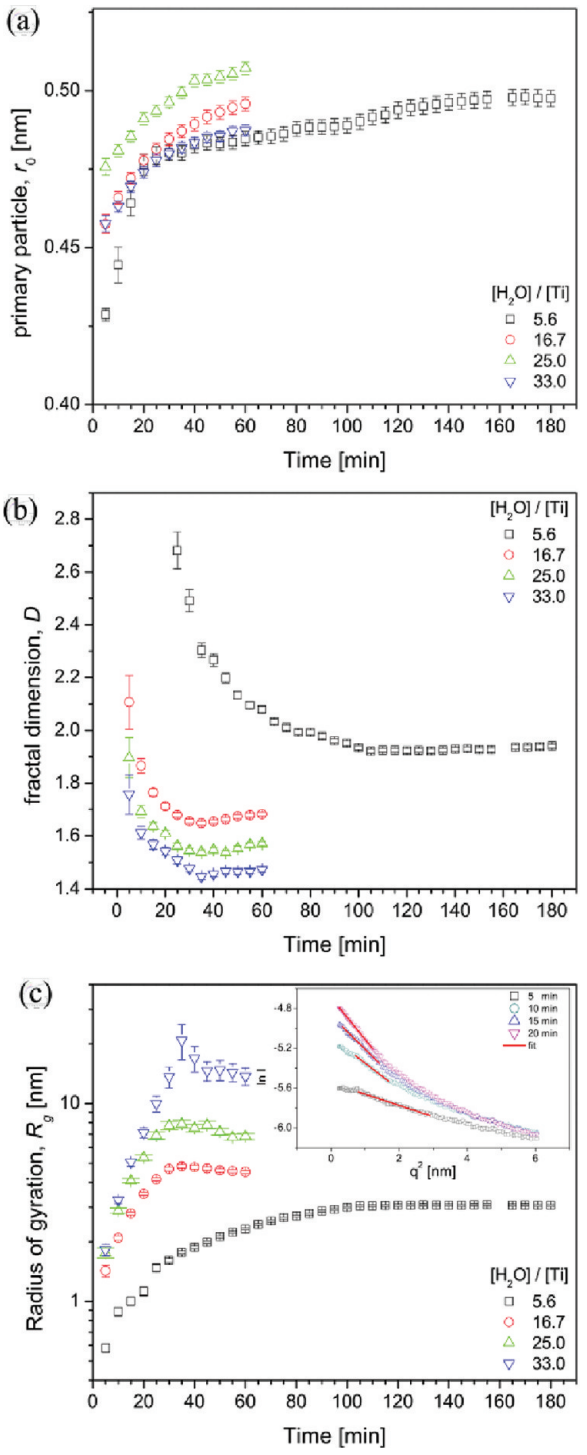

Figure 5. Fitted parameters from mass-fractal structure factor $S_F(q)$ and spherical form factor $P(q)$: (a) primary particle radius, r_0; (b) fractal dimension, D; (c) radius of gyration, R_g. Inset shows scattering data for the first 20 min plotted as ln $I(q)$ vs q^2 for $q < R_g^{-1}$.

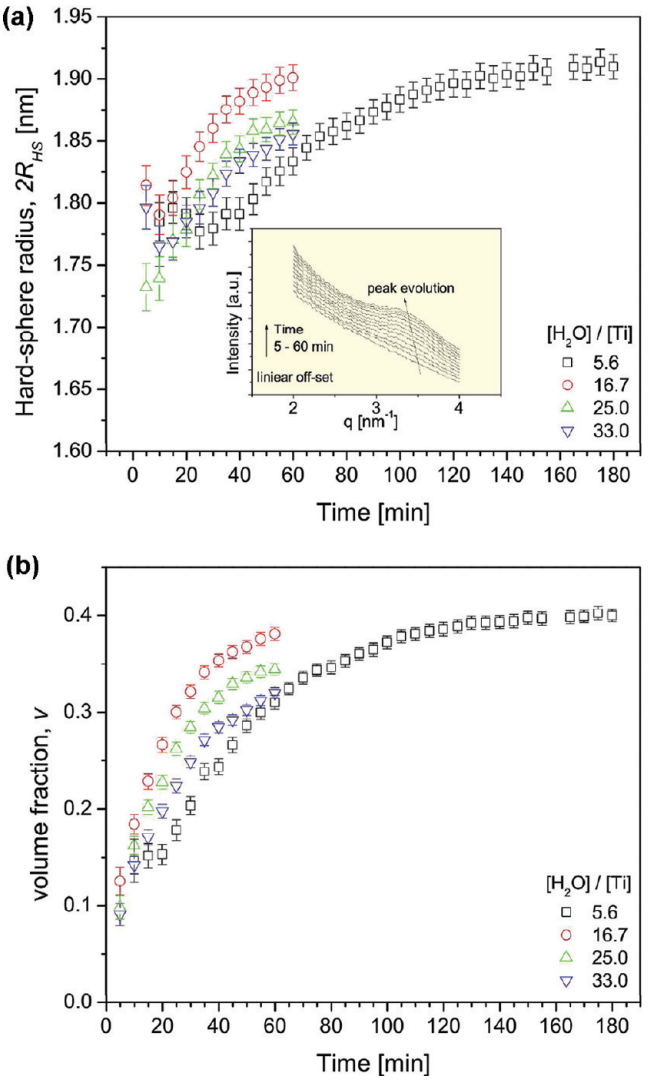

Figure 6. Fitted parameters from correlation structure factor $S_C(q)$: (a) double hard-sphere radius $2R_{HS}$; inset: evolution of correlation peak in corresponding SAXS pattern; (b) evolution of volume fraction, v.

can only be compared within a single time-resolved series of measurements, but general trends can be interpreted. For sols with $[H_2O]/[Ti] > 16$, the overall decrease of $N(\Delta\rho)^2$ was mainly due to the decrease of the contribution from internally correlated structures. The factor $\varepsilon N(\Delta\rho)^2$ remained fairly constant. Initially, $\varepsilon \sim 0.5$. Then, as the reaction progressed, more than 70% of the total intensity prefactor $N(\Delta\rho)^2$ was associated with fractal-like particles. For a sol with lower hydrolysis ratio, i.e., $[H_2O]/[Ti] = 5.6$, the same trend was observed, but slower, with an onset at $t = 25$ min. The scattering curve in the first 20 min can be fitted fairly well by the sphere form factor eq 3, suggesting that the system consisted of isolated spherical primary particles in the earliest stage of development.

4.3. Interpretation of Data. The viscosity measurements indicated that oligomerization and gelation in the hydrolyzed alkoxide−carboxylate precursor of barium titanate was strongly temperature-dependent, with an apparent activation energy of 120 kJ/mol. The question arises with which process or structural feature one can associate this value. The rheological sol−gel transition of barium titanate sols prepared from titanium(IV) *iso*-propoxide in 2-methoxyethanol and barium hydroxide monohydrate in water and methanol also had an activation energy of 120 kJ/mol.[33] However, in that case, neither acetic acid nor barium acetate was used, and gelation occurred at high pH rather than in an acidic medium as in our study. An activation energy of 120 kJ/mol was also measured during the gelation of a TiO_2

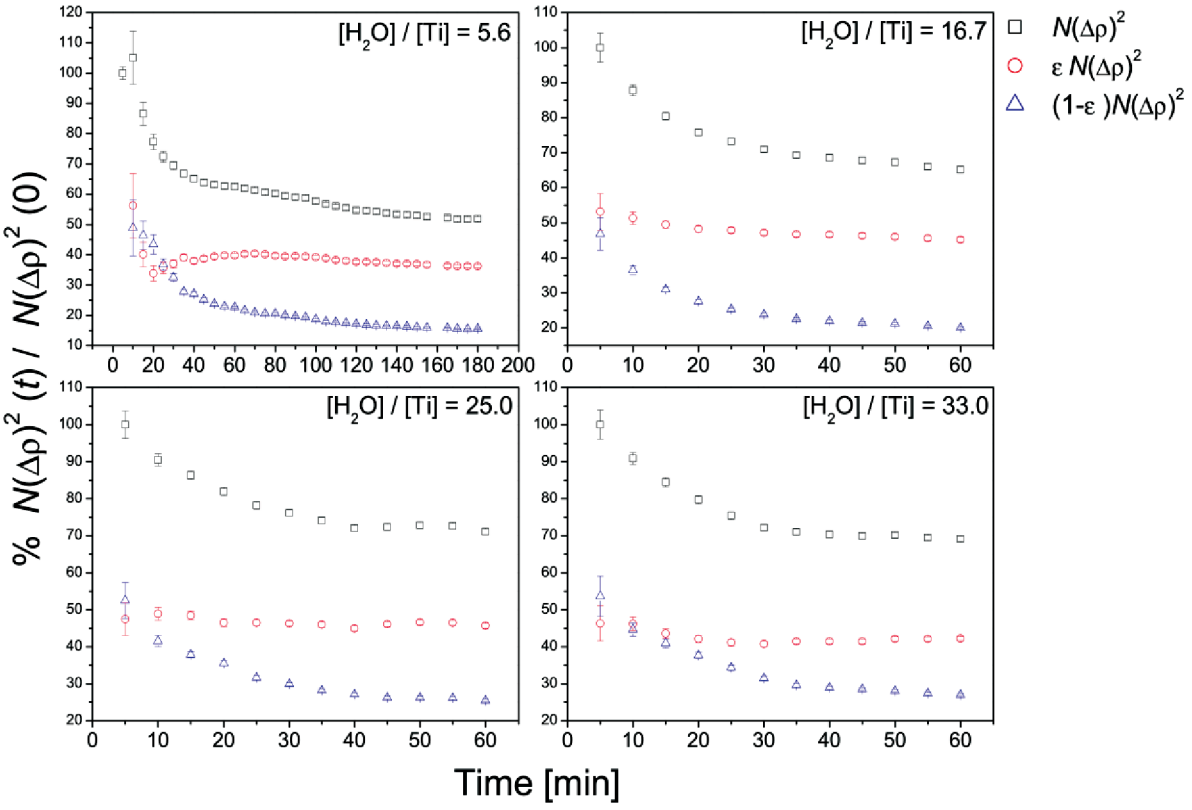

Figure 7. Evolution of $N(\Delta\rho)^2(t)$, contribution of mass fractal-like structures $\varepsilon N(\Delta\rho)^2(t)$, and contribution from internally correlated structures $(1 - \varepsilon)N(\Delta\rho)^2(t)$. All values of $N(\Delta\rho)^2$ were normalized against $N(\Delta\rho)^2$ at t = 5 min of each of the investigated series.

system derived from titanium(IV) *n*-butoxide stabilized with acetylacetone in *n*-butanol[34] and was found to be independent of hydrolysis ratio. Such values of E_a are relatively high. For instance, the activation energy of the sol-to-gel transition of hydrolytic silicate systems is in the range between 40 and 80 kJ/mol,[38] whereas in nonhydrolytic alumina gels it is 80−105 kJ/mol.[39] The value that we found in the present study seems to be associated with the condensation of the Ti precursor, as is similar to the activation energy of pure titanium(IV) *n*-butoxide.

Our analysis showed that the structural evolution of the BTO sol can be divided into three periods: (i) $t/t_g < 0.2$, where neither MFG nor NLG could be applied. SAXS measurements showed the presence of only small isolated primary particles in this period; (ii) $0.2 < t/t_g < 0.8$, where mass fractal-like structures, composed of primary particles, were formed. The SAXS data showed that besides fractal-like structures also other structures with internal correlations were present, in particular from the early stages of sol development in stage (ii); (iii) $0.8 < t/t_g < 0.97$, where higher-order clustering effects, probably cluster−cluster aggregation of the mass fractal-like structures into a larger-scale 3D gel network, occurred.

The primary particles formed in stage (i) were spherical in shape and had a radius of 0.45−0.50 nm. Similar structural motifs have been observed in a number of titania-related gelling systems.[40−43] Titanium(IV) alkoxide-derived clusters, synthesized in reactions with carboxylic acids, are known to yield various geometrical shapes depending on the molar ratio [O]/[Ti] per cluster.[43] For [O]/[Ti] = 1.0, two cluster geometries are known: hexaprismane and octacyclane.[43−46] The latter is a ring structure, built of eight coordination octahedra. Hexaprismane is usually formed in the presence of highly acidic ligands and has an inorganic core $Ti_6(\mu_3\text{-}O)_6$. The diameter of the inorganic core is 0.46 nm, roughly two times smaller than the diameter of our primary scatterers. Larger spherical titanium oxoalkoxide clusters with inorganic cores $Ti_{12}O_{16}$, $Ti_{17}O_{24}$, and $Ti_{18}O_{27}$ are known to form in acetic acid at elevated temperatures.[47] The minor size changes of r_0 observed in our experiments could be attributed to evolution of the ligand environment around the core and/or variations in [O]/[Ti]. It is noted that the outer organic ligand shell surrounding an inorganic core is not directly visible by SAXS because its local electron density is too similar to the electron density of the surrounding solvent phase. The diameter of the cluster including the outer shell is therefore larger than r_0.

Acetic acid acts as a key chelating agent, and its presence suggests the formation of titanium acetates and/or titanium (oxo)alkoxyacetates due to (partial) exchange of alkoxy ligands by acetate. Ti alkoxides in an excess of acetic acid formed a water-soluble precipitate with stoichiometry $TiO(CH_3COO)_2$ at $[CH_3COOH]/[Ti] > 5$ by NMR, FTIR, and EXAFS.[48] The coordination number of Ti in the precipitate was 6; all alkoxy groups were removed; and acetate ligands were found in the bridging positions. The clusters were oligomeric in nature, and Ti−Ti correlations of 3.12 Å were shown by EXAFS. The chemical composition of the precipitated product was independent of the alkoxy group. On the other hand, it is known that complexation of Ti-alkoxides by carboxylates is disadvantageous at elevated temperatures because practically all acid involved in the reaction is transformed into esters and water.[47] This shows that no straightforward conclusions can be drawn on the structure of Ti-oxoclusters based only on reaction conditions.

dx.doi.org/10.1021/jp206572q | *J. Phys. Chem. C* 2011, 115, 20449–20459

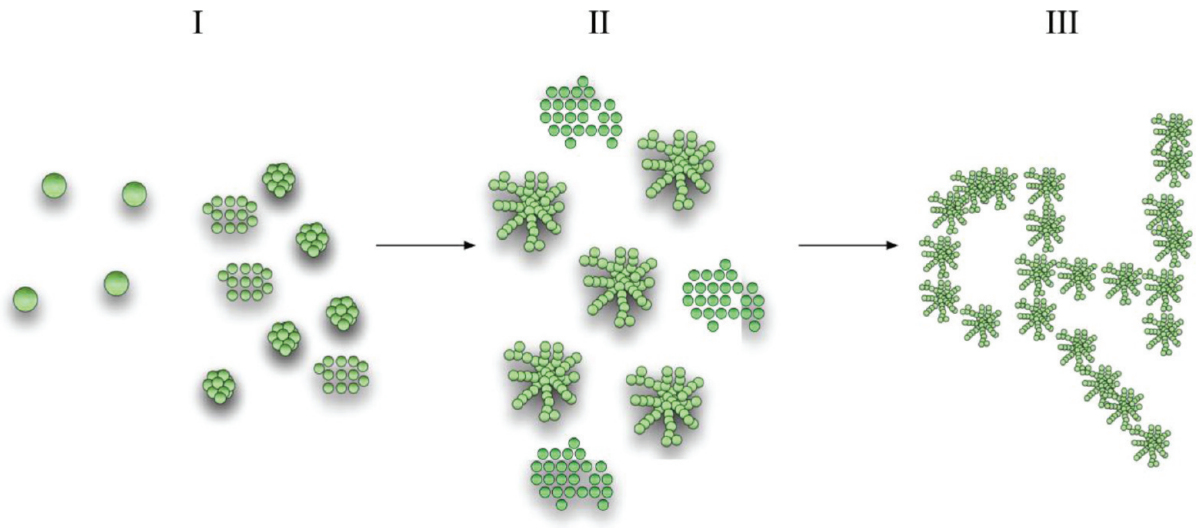

Figure 8. Schematic representation of the sol−gel process of BTO precursor sols. (I) Induction stage: formation of monodisperse spherical primary particles with an inorganic core diameter $2r_0$ = 0.9 nm and an outer organic ligand shell of ∼0.45 nm thickness ($R_{HS} - r_0$). (II) Growth of branched oligomeric structures and increasing packing density in agglomerates of titania nanoparticles of very similar size. (III) Cluster−cluster aggregation of fractal-like titania oligomers into a 3D macroscopic gel of low density, in which each constituent titania oligomer has a limited number of direct neighbors, i.e., just above 2 on average.

Simple mixing experiments showed that titanium *iso*-propoxide in 2-methoxethanol indeed formed a precipitate in an excess of acetic acid when no external water was added. However, in the presence of barium acetate, precipitation occurred after an approximately ten times longer period than when barium was absent. When water was also added to the system, no precipitation occurred, but gelation was observed instead, as the SAXS and viscosity measurements showed. Apparently, the as-formed titanium (oxo)alkoxyacetate clusters[48] were hydrolyzed by water and condensed into a gel. Our observations show that the presence of barium ions somehow influences the reaction scheme between alkoxide and acetate ligands in Ti-based clusters and oligomers, suppressing the rapid formation of Ti-based precipitates. The SAXS data provide no indication that Ba ions are structurally associated with as-formed Ti clusters, and it is indeed known that barium ions do not easily participate in coordination complexes. However, the interaction could also be indirect. For instance, the presence of divalent barium ions affects the ionic strength of the solution significantly, and this influences the screening of charges in solution, thereby changing the ionic interactions and reactivity of charged species present in solutions. However, it is stressed that several alternative explanations between which we cannot discriminate based on the current experimental evidence are also possible.

The evolution of D and R_g in the fractal-like structures in stage (ii) was clearly dependent on hydrolysis ratio. Lower ratios yielded smaller agglomerates with higher D. The obtained values of D and R_g are typical for various TiO_2 gelling precursor systems.[42,49,50] The actual structures in solution that yield scattering patterns that can be described best in terms of a fractal structure are most likely branched oligomers, composed of the type of primary scatterers discussed above. As can be seen in Figure 4B and 4C, R_g reaches a maximum and D a minimum value after ∼30 min. After that D increases slightly, and R_g decreases. Although it cannot be ruled out completely that the trend is influenced to a small degree by the increasing error in the determination of ξ, it is plausible that it presents an actual physical process. Possibly, it is an effect of syneresis, a process in which a polymeric particle or network contracts spontaneously under the influence of ongoing condensation, thereby expelling liquid from the spaces between the polymer segments.[51] Syneresis is expected to result in smaller particles with a higher D value, in agreement with the experimental data for the highest hydrolysis ratios. An alternative explanation is that the fractal-like Ti-based oligomers, which form relatively low density structures at high hydrolysis ratios, merge with each other at this point, leading to reconfiguration and compaction of these structures. Since the factor $\varepsilon N(\Delta\rho)^2$ remained more or less constant in time for all investigated samples, the change of N and $\Delta\rho$ over the course of reaction was probably negligible.

For the structures with internal correlations, we found that the hard-core radius R_{HS} hardly increased, but the volume fraction v increased by a factor of ∼4. This means that the primary hard sphere scatterers remained very similar in size, but they reorganized in the course of the process, increasing their internal degree of packing considerably. The hard sphere radius R_{HS} was ∼0.9 nm and was based on the mutual spacing between scattering entities. Since we think that these hard sphere scatterers have the same physical origin as the primary scatterers in the fractal-like structures, where r_0 = 0.45 nm, this means that the outer organic ligand shell has an estimated thickness $R_{HS} - r_0 \sim$ 0.45 nm. So the internally correlated structures are probably ordered agglomerates of Ti-based clusters. Given the fact that the experimental correlation peak in the SAXS patterns had a distinct maximum, it seems that these Ti-based clusters must be very similar in size. The overall size of these ordered agglomerates cannot be determined from the experimental data. They must be smaller than the wavelength of visible light, because the solutions were completely transparent in the visible range. The contribution of these structures to the total X-ray scattering intensity of the system decreased in the course of the reaction, as expressed by the factor $(1 - \varepsilon)N(\Delta\rho)^2$ in Figure 7. The effect is most likely related to a decrease of scattering contrast $\Delta\rho$, possibly due to the increased packing density observed in these species.

The evolution of $\varepsilon N(\Delta\rho)^2(t)$ and $(1-\varepsilon)N(\Delta\rho)^2(t)$ showed that both fractal-like structures and structures with internal correlations had already formed at the beginning of stage (ii). In our model, we assume that these structures are constructed from the same primary particles. Hence, a common form factor $P(q)$ was used. We found that the radii r_0 of these primary scatterers increased by about 10% in the course of the experiment. Our model does not include scattering interactions between fractal-like structures and internally correlated structures, i.e., interactions between branched titania oligomers and packed agglomerates. Attempts to fit the experimental data with a model that included such effects were not successful. Hence, it was concluded that these two types of structures do not interact physically on the agglomerate level. Probably they are located in spatially different regions of the sol.

5. CONCLUSIONS

The BTO precursor sols investigated here consist of titanium-based oligomeric structures and Ti-based agglomerates of nanoparticles of similar size. Barium remains dissolved in acetic acid and was seen to suppress rapid formation of a titanium-rich precipitate from solution. The structural evolution of the titania nanostructures could be monitored by SAXS and viscosity measurements and involves three phases: (i) formation of isolated primary scatterers and very small agglomerates of such scatterers (induction), (ii) growth of branched oligomeric mass fractal-like structures, in parallel to agglomerates of primary scatterers of very similar constant size that increase their packing density, and (iii) gelation. The contribution to the total scattering intensity of the nonfractal-like agglomerates decreases in the course of stage (ii) to less than 20%, so the gelation process occurs mainly due to the aggregation of fractal-like oligomers. The microstructure of these fractal-like titania oligomers depends on hydrolysis conditions. The overall scheme of the sol−gel process based on the SAXS and viscosity data presented in this paper is shown in Figure 8.

AUTHOR INFORMATION

Corresponding Author

*E-mail: j.e.tenelshof@utwente.nl. Phone: +31 53 489 2695. Fax: +31 53 489 2990.

ACKNOWLEDGMENT

This work was financially supported by The Netherlands Technology Foundation STW. We thank The Netherlands Organization for Scientific Research (NWO) for providing us with beam time at the ESRF DUBBLE beamline. Beamline staff of DUBBLE are thanked for their competent support.

REFERENCES

(1) Yoon, D. *J. Ceram. Proc. Res.* **2006**, *7*, 343–354.
(2) Pithan, C.; Hennings, D. H.; Waser, R. *Int. J. Appl. Ceram. Technol.* **2005**, *2*, 1–14.
(3) Phule, P. P.; Risbud, S. H. *J. Mater. Sci.* **1990**, *25*, 1169–1183.
(4) Schwartz, R. W.; Schneller, T. S.; Waser, R. *C. R. Chim.* **2004**, *7*, 433–461.
(5) Schwartz, R. W.; Narayanan, M. Chemical Solution Deposition—Basic Principles. In *Solution Processing of Inorganic Materials*; Mitzi, D.B., Ed.; John Wiley & Sons, Inc.: NJ, 2009; pp 33−76.
(6) Huffman, M. *Integr. Ferroelectr.* **1995**, *10*, 39–53.
(7) Phule, P. P.; Risbud, S. H. *Adv. Ceram. Mater.* **1988**, *3*, 183–185.
(8) Schwartz, R. W. *Chem. Mater.* **1997**, *9*, 2325–2340.
(9) Schwartz, R. W.; Boyle, T. J.; Lockwood, S. J.; Sinclair, M. B.; Dimos, D.; Buchheit, C. *Integr. Ferroelectr.* **1995**, *7*, 259–277.
(10) Yi, G.; Sayer, M. *Ceram. Bull.* **1991**, *70*, 1173–1179.
(11) Assink, R. A.; Schwartz, R. W. *Chem. Mater.* **1993**, *5*, 511–517.
(12) Hasenkox, U.; Hoffmann, S.; Waser, R. . *J. Sol-Gel Sci. Technol.* **1995**, *12*, 67–79.
(13) Hoffmann, S.; Waser, R. *J. Eur. Ceram. Soc.* **1999**, *19*, 1339–1343.
(14) Frey, M. H.; Payne, D. A. *Chem. Mater.* **1995**, *7*, 123–129.
(15) Hennings, D.; Rosenstein, G.; Schreinemacher, H. *J. Eur. Ceram. Soc.* **1991**, *8*, 107–115.
(16) Guinier, A.; Fournet, G. *Small Angle Scattering of X-rays*; John Wiley & Sons Inc.: New York, 1955.
(17) Kratky, O. A Survey. In *Small Angle X-ray Scattering*; Glatter, O., Kratky, O., Ed.; Academic Press: London, 1982; pp 3−13.
(18) Porod, G. General theory. In *Small Angle X-ray Scattering*; Glatter, O., Kratky, O., Ed.; Academic Press: London, 1982; pp 17−52.
(19) Craievich, A. F. *Mater. Res.* **2002**, *5*, 1–11.
(20) Pedersen, J. S. *Adv. Colloid Interface Sci.* **1997**, *70*, 171–210.
(21) Squires, G. L. *Introduction to the Theory of Thermal Neutron Scattering*; Cambridge University Press: Cambridge, U. K., 1978.
(22) Sorensen, C. M. *Aerosol Sci. Technol.* **2001**, *35*, 648–687.
(23) Teixeira, J. *J. Appl. Crystallogr.* **1988**, *21*, 781–785.
(24) Freltoft, T.; Kjems, J. K.; Sinha, S. K. *Phys. Rev. B* **1986**, *33*, 269–275.
(25) Berry, M. V.; Percival, I. C. *Opt. Acta* **1986**, *33*, 577–591.
(26) Pontoni, D.; Narayanan, T.; Petit, J.-M.; Grübel, G.; Beysens, D. *Phys. Rev. Lett.* **2003**, *90* (188301), 144–145.
(27) Percus, J. K.; Yevick, G. J. *Phys. Rev.* **1958**, *110*, 1–13.
(28) Vrij, A. *J. Chem. Phys.* **1979**, *71*, 3267–3270.
(29) Baxter, R. J. *J. Chem. Phys.* **1968**, *49*, 2770–2774.
(30) Marquardt, D. *SIAM J. Appl. Math.* **1963**, *11*, 431–444.
(31) Bras, W.; Dolbnya, I. P.; Detollenaere, D.; van Tol, R.; Malfois, M.; Greaves, G. N.; Ryan, A. J.; Heeley, E. *J. Appl. Crystallogr.* **2003**, *36*, 791–794.
(32) Pope, E. J. A.; Mackenzie, J. D. *J. Non-Cryst. Solids* **1988**, *101*, 198–212.
(33) Brasseur, A.; Michaux, B.; Pirard, R.; Cantfort van, O.; Pirard, J. P.; Lecloux, A. J. *J. Sol-Gel Sci. Technol.* **1997**, *9*, 5–15.
(34) Ponton, A.; Barboux-Doeuff, S.; Sanchez, C. *Colloids Surf. A* **2000**, *162*, 177–192.
(35) Flory, P. J. *J. Am. Chem. Soc.* **1943**, *65*, 372–382.
(36) Bechtold, M. F.; Vest, R. D.; Plambeck, L., Jr. *J. Am. Chem. Soc.* **1968**, *90*, 4590–4598.
(37) Bechtold, M. F.; Mahler, W.; Schunn, R. A. *J. Polym. Sci., Polym. Chem.* **1980**, *18*, 2823–2855.
(38) Scherer, G. W. *J. Ceram. Soc. Jpn.* **1987**, *95*, 21–44.
(39) Grader, G. S.; Hazan, de, Y.; Cohen, Y.; Bravo-Zhivotovskii, D. *J. Sol-Gel Sci. Technol.* **1997**, *10*, 5–12.
(40) Jalava, J. - H.; Hiltunen, E.; Kähkönen, H.; Erkkilä, H.; Härmä, H.; Taavitsainen, V. − M. *Ind. Eng. Chem. Res.* **2000**, *39*, 349–361.
(41) Torma, V.; Peterlik, H.; Bauer, U.; Rupp, W.; Husing, N.; Bernstorff, S.; Steinhart, M.; Goerigk, G.; Schubert, U. *Chem. Mater.* **2005**, *17*, 3146–3153.
(42) Pattier, B.; Henderson, M.; Brotons, G.; Gibaud, A. *J. Phys. Chem. B* **2010**, *114*, 5227–5232.
(43) Rammal, A.; Brisach, F.; Henry, M. *C. R. Chim.* **2002**, *5*, 59–66.
(44) Papiernik, R.; Hubert-Pfalzgraf, L. G.; Vaissermann, J.; Heriques Baptista Goncalves, M. C. *J. Chem. Soc., Dalton Trans.* **1998**, *14*, 2285–2287.
(45) Sui, R.; Charpentier, A. S.; Rizkalla, A. S.; Jennings, M. C. *Acta Crystallogr.* **2006**, *E62*, m373–m375.
(46) Boyle, T. J.; Alam, T. M.; Tafoya, C. J.; Scott, B. L. *Inorg. Chem.* **1998**, *37*, 5588–5594.
(47) Rozes, L.; Sanchez, C. *Chem. Soc. Rev.* **2011**, *40*, 1006–1030.

(48) Doeuff, S.; Henry, M.; Sanchez, C. *Mater. Res. Bull.* **1990**, *25*, 1519–1529.
(49) Kamiyama, T.; Mikami, M.; Suzuki, K. *J. Non-Cryst. Solids* **1992**, *150*, 157–162.
(50) Blanchard, J.; Ribot, F.; Sanchez, C.; Bellot, P. − V.; Trokiner, A. *J. Non-Cryst. Solids* **2000**, *265*, 83–97.
(51) Brinker, C. J.; Scherer, G. W. *Sol-gel science: The Physics and Chemistry of Sol-Gel Processing*; Academic Press: New York, 1990; p 374.